CrossMark

Effect of grain refinements on the microstructure and thermal behaviour of Mg–Li–Al alloy

Mariusz Król[1] (iD)

Abstract

The light as-cast Mg–9Li–1.5Al alloys were manufactured and modified by 0.2 mass% Zr, commercial 0.2 mass% TiBor and 0.2 mass% AlSr master alloys. The thermal derivative analysis using UMSA platform was utilised to characterise a crystallisation process. Samples were heated up to 700 °C and then freely cooled down (~ 0.6 °C s^{-1}) to ambient temperature in order to simulate the natural cooling of casts. Dilatometry study was used to identify changes in solid state. The relative elongation of unmodified and modified alloys was measured in the temperature range from 20 to 400 °C, with a heating rate 1.0 °C s^{-1}. The effects of Zr, TiBor and AlSr content on the microstructure of analysed magnesium alloys were investigated. Evaluation of microstructure was identified by light microscope, scanning electron microscopy, X-ray diffraction and energy-dispersive X-ray spectroscopy. The results showed that the addition of TiBor reduced the grain size of Mg–9Li–1.5Al cast alloy from 930 to 530 μm, while the addition of AlSr master alloy reduced the grain size to 480 μm. Moreover, an addition of TiBor and AlSr simultaneously reduced the grain size to 430 μm. The addition of Zr causes a reduction in grain size to 630 μm. The addition of grain refinement causes changes in crystallisation process and variations in the coefficient of linear thermal expansion (CTE).

Keywords Magnesium–lithium alloys · Thermal expansion · Thermal derivative analysis · Grain refinement

Introduction

Following the World War II, Mg–Li-based alloys, as an emerging light structural metallic material, have been presumed to be extensively used in aerospace and civilian areas, such as transport, electronics packaging and sports manufacturing for their high specific strength and specific stiffness, excellent damping and electromagnetic shielding properties [1, 2].

In the beginning, the analysis of Mg–Li-based alloys and composites including applications, microstructures, mechanical properties and processing technologies was regularly presented. Furthermore, the development in the research of intermetallic particles reinforced Mg–Li matrix composites was studied [3, 4].

Mg–Li-based alloys are the lightest among the magnesium alloys and serve as the important structural materials for aerospace industry. They maintain high cold formability, and the problems of magnesium–lithium binary alloys, such as poor resistance to corrosion and low strength, limit their utilisation [5].

There are few standard ways to enhance the strength of metallic materials through decreases in grain size and can be divided into two groups like thermal and chemical methods. The thermal method of grain refinement is superheating, and chemicals are zirconium, carbon, silicon carbide, manganese, titanium, calcium, strontium, antimony, cerium additions and Elfinal process [6, 7].

The additional methods capable of raising the strength are an addition of alloying elements. The increase in a third element—for example aluminium—to Mg–Li-based alloys serves to change the strength relating to intermetallic particle formation [1, 3].

The mechanical properties of Mg–Li alloys increase apparently with the addition of Al content, during the elongation of alloys reduces dangerously when the Al

✉ Mariusz Król
  mariusz.krol@polsl.pl

1 Institute of Engineering Materials and Biomaterials, Faculty of Mechanical Engineering, Silesian University of Technology, Konarskiego 18a St., 44-100 Gliwice, Poland

content is higher than 6 mass%. Titanium, strontium and zirconium are also a useful alloying element to improve Mg–Li properties [2, 6].

According to the Mg–Li binary phase diagram, if the Li content is less than around 5.5 mass%, the metal is formed of a single α(Mg) phase with hcp structure. When the Li content is within 5.5 and 11 mass%, the hcp α(Mg) phase coexists with bcc-structured β(Li) phase, while the structure has only a single bcc-structured β(Li) phase when the Li content is higher than 11 mass% [8, 9].

Nucleation of the primary phase is the initial step in the transition of molten alloys into the solid state. Nucleation control has been the subject of many studies [10, 11]. In the case of Mg alloys, a finer grain size increases most mechanical properties, including yield strength due to the high Hall–Petch coefficient, corrosion resistance and creep resistance [12–15].

In this study, the ternary alloys Mg–9Li–1.5Al (mass%) were manufactured and modified by processed by commercial Zr, TiBor and AlSr master alloys. The microstructure evolution, thermal derivative analysis, dilatation, scanning electron microscopy, X-ray diffraction and energy-dispersive X-ray spectroscopy techniques were used to examine the effect of grain refinements.

Experimental

Within the framework of the present work, alloys of magnesium with lithium and aluminium and with Zr, TiBor and AlSr as grain refinement have been melted, casted and examined. The raw materials used in these experiments were magnesium with technical grade (min. 99.5% Mg), aluminium 3N8 (99.98% Al), lithium (99.9% Li), TiBor, AlSr and Zr as refinements were utilised. Melting and casting of alloys were carried out using laboratory vacuum induction furnace VSG 02 from the company Balzers. Melts held in a crucible of Al_2O_3 in shape of ø 60 mm × 80 mm, using the ceramic material sheath thermocouple for measuring the temperature of melting and casting alloys. Melting temperature was approx. 700/720 °C and the melting time approx. 5 min., which, taking into account the strong bath stirring electrodynamic eddy currents in enough for the complete homogenisation of the melt. Grain refinement was introduced at the end of the melting process from the vacuum containers. After placed of grain refinement in the alloy, melts kept in the liquid state for 2 min, followed by the casting. The chemical composition of analysed Mg–Li–Al alloys and used grain refinements are given in Tables 1 and 2.

The linear thermal expansion coefficient of the investigated magnesium–lithium–aluminium alloys was measured in argon atmosphere using the Bahr 805A/D dilatometer

Table 1 Chemical compositions of analysed Mg–Li–Al alloys

Elements/mass%

Li	Al	Zr	TiBor	AlSr10	Mg
9	1.5	–	–	–	Balance
9	1.5	0.2	–	–	Balance
9	1.5	–	0.2	–	Balance
9	1.5	–	–	0.2	Balance
9	1.5	–	0.2	0.2	Balance

Table 2 Chemical composition of grain refinements

	Element	mass%
TiBor	Ti	4.9
	B	0.95
	Fe	0.17
	Si	0.06
	V	0.09
	Al	Balance
AlSr10	Sr	10.07
	Fe	0.13
	Si	0.08
	Ca	< 0.10
	Al	Balance

over a temperature range from ambient temperature to 400 °C at heating and cooling rates of 1 °C s^{-1}. The thermocouple type S was utilised to measure changes in temperatures. Cylindrical samples in shape 10 mm in length and 4 mm in diameter were used in dilatometry test.

The thermal derivative analysis (TDA) was done on the prepared cylindrical samples in shape of 18 mm in diameter and 20 mm using UMSA device [10, 11, 14]. Samples were melted at 700 °C in an argon atmosphere. Following isothermal holding for 90 s, all the melts were solidified and cooled to ambient temperature in the crucibles with argon protection in the furnace to minimise the oxidation.

The signal from the thermal derivative analysis was acquired using a high-speed National Instruments data acquisition system. The recorded data were analysed in Fityk software. The cooling curves and corresponding derivative curves were plotted to define thermal events, based on the first and second derivative of cooling curve. The test samples were solidified at an average cooling rate of approximately 0.6 °C s^{-1} in the range of liquidus and solidus temperature. The cooling rate was determined using the following formula:

$$CR = \frac{T_{liq} - T_{sol}}{t_{sol} - t_{liq}}$$

where T_{liq} and T_{sol} are the liquidus and solidus temperatures, respectively, and t_{liq} and t_{sol} the times from the cooling curve that correspond to liquidus and solidus temperatures, respectively.

The Newtonian method was applied in this research to determine the baseline. This means that the thermal gradient across the specimen is considered to be zero and that heat transfer between the casting and the mould occurs through convection. The Fourier method is another method used to calculate the baseline in which the positions of two thermocouples at the beginning and end of the solidification process are considered. However, it is much more complicated than the Newtonian method. Besides, a thermal contraction of the metal occurs during solidification, the exact positions of the two-thermocouple tips are difficult to estimate [16–18]. The base line has been predicted by the sixth polynomial fitting $(dT/dt)_{BL} = a_0 + a_1T + a_2t)_{BL} = a_0 + a_1T + a_2T^2 + a_3T^3 + a_4T^4 + a_5T^5 + a_6T^6$ between the beginning and the end of solidification in the first derivative curve. The sixth-order polynomial yields a correlation coefficient greater than 0.97.

Metallographic specimens were horizontally sliced at the position that is 10 mm from the top. The as-cast grains of the etched samples were measured using polarised light in optical microscope Leica equipped Q-WinTM image analyser. The grain size was determined by the linear intercept method at the centre of transverse sections.

The X-ray qualitative and quantitative microanalysis and the analysis of a surface concentration of cast elements in the examined magnesium–lithium–aluminium unmodified and modified alloys have been made on the scanning electron microscope ZEISS SUPRA 35 with a system EDAX XM4 TRIDENT consisting of spectrometer EDS, WDS and EBSD (20 kV, 15 mm of work distance and 30 μm of aperture).

Phase composition was determined by the X-ray diffraction technique utilising the X'Pert apparatus including a cobalt lamp with 40 kV voltage. The calculation was done by angle range of 2Θ: 30°–110°. The

measurement step was 0.03° in length while the pulse counting time was 30 s.

Hardness tests were made using Zwick ZHR 4150 TK hardness tester in the HRF scale.

Results and discussion

The analysis of coefficient of linear thermal expansion of Mg–9Li–1.5Al (Table 3 and Fig. 1) has validated the fact that CTE depends on temperature. Untreated Mg–9Li–1.5Al alloy has CTE about $29.4 \cdot 10^{-6}$ K^{-1}, and with further increase in temperature to 250 °C, CTE increases to $34.3 \cdot 10^{-6}$ K^{-1}. Further increase in temperature to 400 °C caused a decrease in CTE to $31.9 \cdot 10^{-6}$ K^{-1}. Analysis of the heating and cooling dilatometric curves of analysed materials modified by TiBor and AlSr is characterised by a linear decrease in linear expansion coefficient as a function of temperature. Moreover, based on changes in elongation during heating and cooling cycle, it was found that shape of
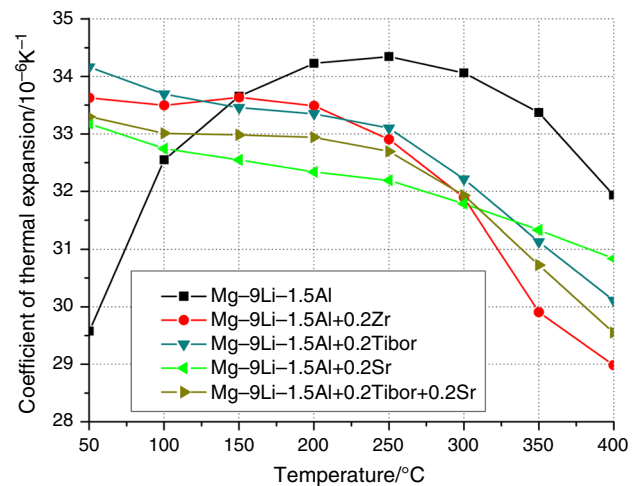

Fig. 1 Changes in coefficient of thermal expansion versus temperature of analysed Mg–Li–Al alloys

Table 3 Resume of thermophysical parameters of Mg–Li–Al alloys after dilatometry analysis

Material	Linear coefficient of thermal expansion $\alpha/10^{-6}$ K^{-1}								Max change in length/mm
	50	100	150	200	250	300	350	400	
Mg–9Li–1.5Al	29.5	32.5	33.6	34.2	34.3	34.0	33.3	31.9	1.205
Mg–9Li–1.5Al+0.2Zr	33.6	33.4	33.5	33.5	32.9	31.8	29.8	28.9	1.086
Mg–9Li–1.5Al+0.2TiBor	34.0	33.6	33.4	33.3	33.0	32.2	31.1	30.1	1.127
Mg–9Li–1.5Al+0.2Sr	33.2	32.5	32.4	32.3	32.1	31.7	31.3	30.8	1.156
Mg–9Li–1.5Al+0.2TiBor+0.2Sr	32.7	32.9	32.9	32.8	32.6	31.9	30.7	29.5	1.108

graphs has a linear relationship that means no transitions in solid state occur.

The phase composition of the investigated alloys treated by grain refinements and untreated was examined by XRD technique. The XRD profile of unmodified alloy demonstrates that there are two phases—β(Li) phase (matrix phase, a solid solution of magnesium in body-centred cubic (bcc) lithium lattice) and α(Mg) phase (solid solution of lithium in hexagonal close-packed (hcp) magnesium lattice), which is faithful with the observation using a light microscope. No peaks of Al including phase are noticed that suggests most of Al exists in a solid solution state. However, with the addition of Zr, new peaks correspond to the Zr phases. Furthermore, with the addition of TiBor and AlSr, no additional peaks were observed.

Optical micrographs of Mg–9Li–1.5Al cast alloy and after modification by Zr, TiBor and AlSr are given in Fig. 2. It can be observed that the structure of the analysed alloys is fundamentally formed of light grey α(Mg) phase and dark grey β-Li phase, which is in consistent with the Mg–Li binary system [8, 9]. Most of the α(Mg) phase is elongated ribbon-like, where β(Li) phase fills the area between α(Mg) phase grains, separated by boundaries between two phases. In the duplex phase matrix, the ratio of α and β phases is 40/60. There also exists some particle-like (Fig. 2e—marked in white circle) phase in the alloy. The granular-dispersive phase of the intermetallic compounds is randomly spread in the α and β matrices. Darker particles have most probably resulted from the aluminium addition in the form of η(LiAl) phase as suggested in
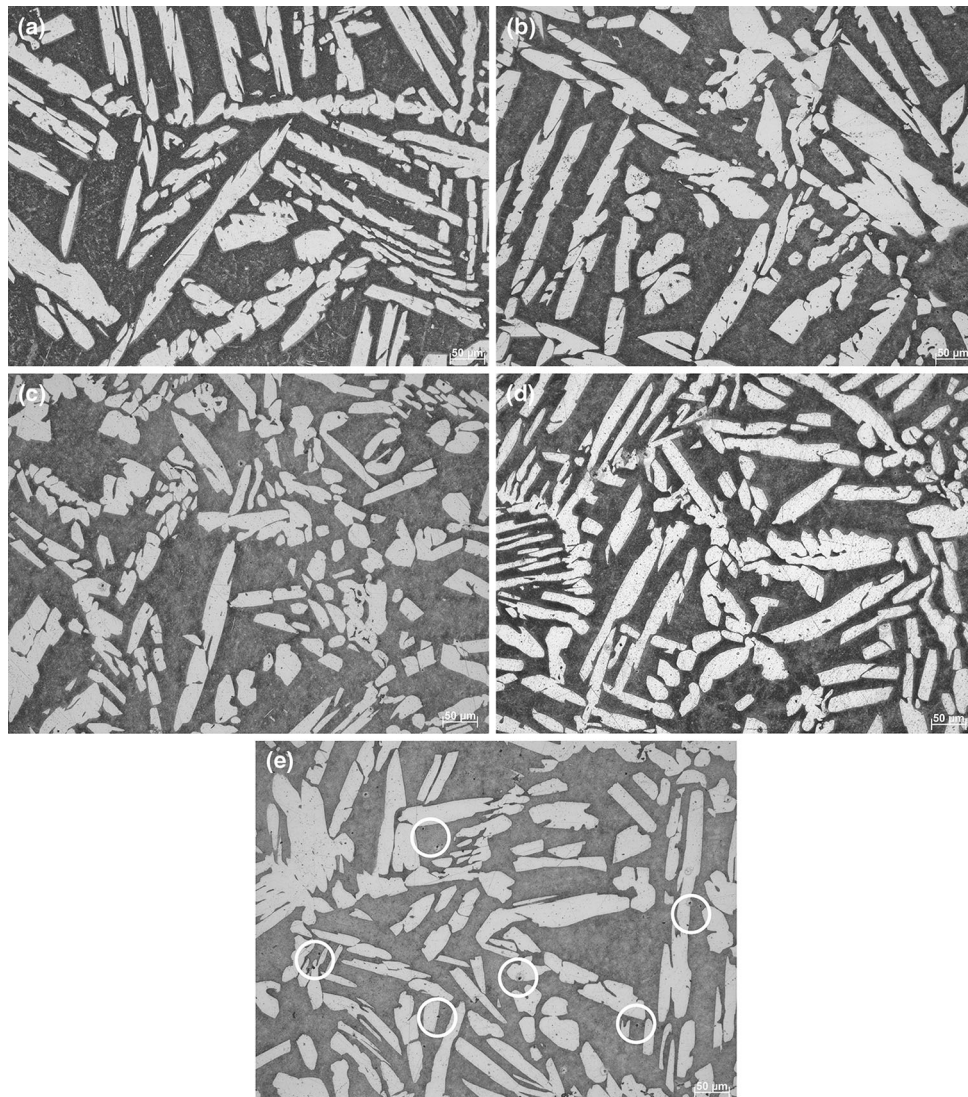

Fig. 2 Optical microstructure of as-cast and after modification of Mg–9Li–1.5Al alloy: **a** Mg–9Li–1.5Al, **b** Mg–9Li–1.5Al+0.2Zr, **c** Mg–9Li–1.5Al+0.2TiBor, **d** Mg–9Li–1.5Al+0.2Sr, **e** Mg–9Li–1.5Al+0.2TiBor+0.2Sr

[8, 9, 19, 20]. SEM analysis of marked circles shows high concentration of Al, indicating that it is η(LiAl) phase. Moreover, the addition of grain refinements effects in the conversion of the elongated-striped α(Mg) phase with a blocky structure and rounded corners. Moreover, optical metallography indicated fully dense alloys.

Analysis of grain size of analysed alloys after thermal derivative analysis cooled at a rate of 0.6 °C s^{-1} appointed by the method of linear interception length shows that the grain refining appearance is different for each alloy (Figs. 3 and 4). Once Zr is added, there is a significant reduction in grain size. The Mg–9Li–1.5Al alloy was refined from 930 to 640 μm by 0.2 mass% Zr. The results showed that the addition of TiBor master alloy decreased the grain size of Mg–9Li–1.5Al cast alloy to 500 μm, while the addition of AlSr master alloy reduced the grain size to 480 μm.

Moreover, an addition of TiBor and AlSr simultaneously reduced the grain size to 430 μm. The relatively small grain size of Mg–9Li–1.5Al+0.2TiBor+0.2Sr is not obviously reflected in its hardness related to Mg–9Li–1.5Al+0.2TiBor. It can be noted that addition of AlSr refiner slightly increases in hardness. In general, the hardness did not increase with TiBor and Zr addition (Fig. 5).

Furthermore, investigated alloys were characterised by SEM equipped with EDS and computer-controlled imaging system. The SEM images of analysed Mg–Li–Al alloys point out dark grey and grey areas relating to the β(Li) phase and α(Mg) phase, respectively, as shown in Fig. 6a. Because lithium is invisible in SEM image, β-phase is darker. Grain refinement of analysed magnesium–lithium–aluminium alloy by 0.2 mass% Zr causes appearance to
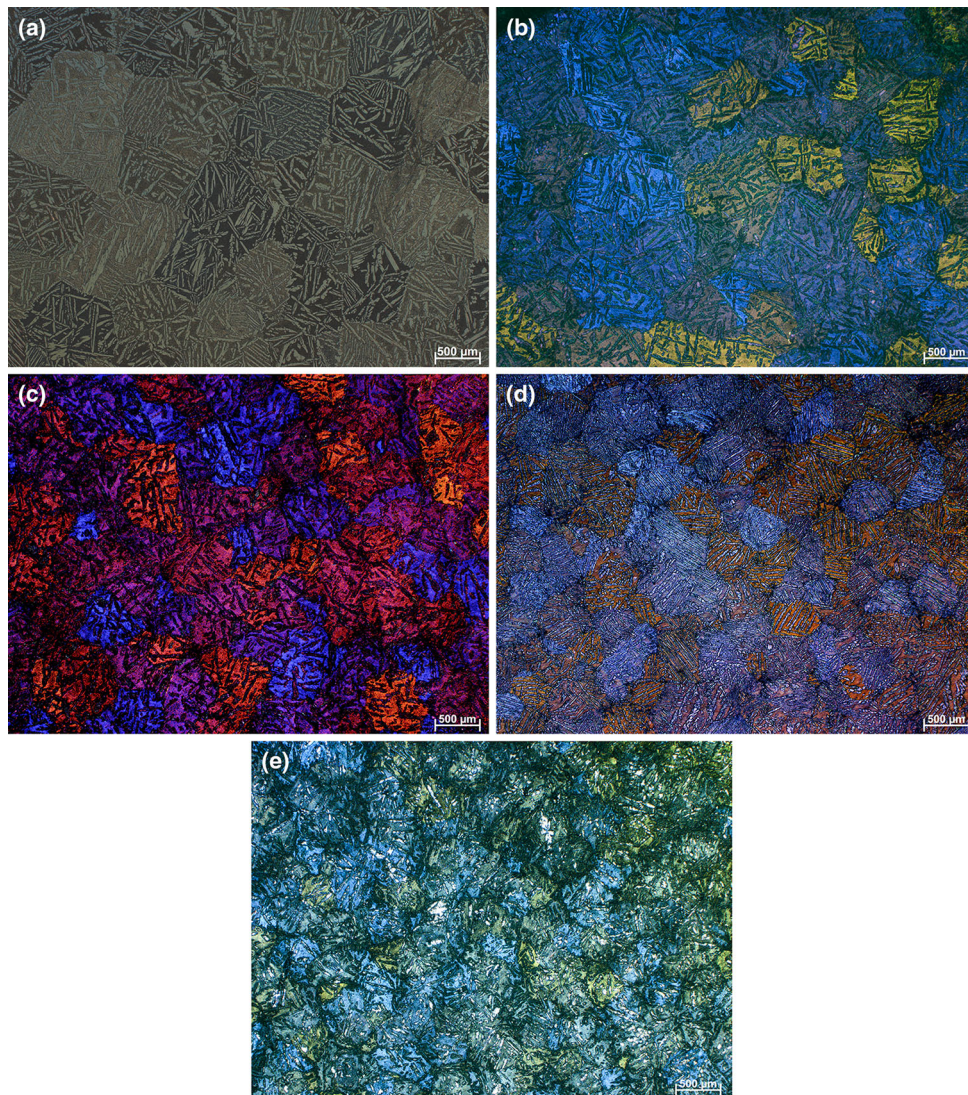

Fig. 3 Microstructure of the grain size for Mg–9Li–1.5Al base alloy at various addition of grain refinements: **a** Mg–9Li–1.5Al, **b** Mg–9Li–1.5Al+0.2Zr, **c** Mg–9Li–1.5Al+0.2TiBor, **d** Mg–9Li–1.5Al+0.2Sr, **e** Mg–9Li–1.5Al+0.2TiBor+0.2Sr, Nomarski contrast
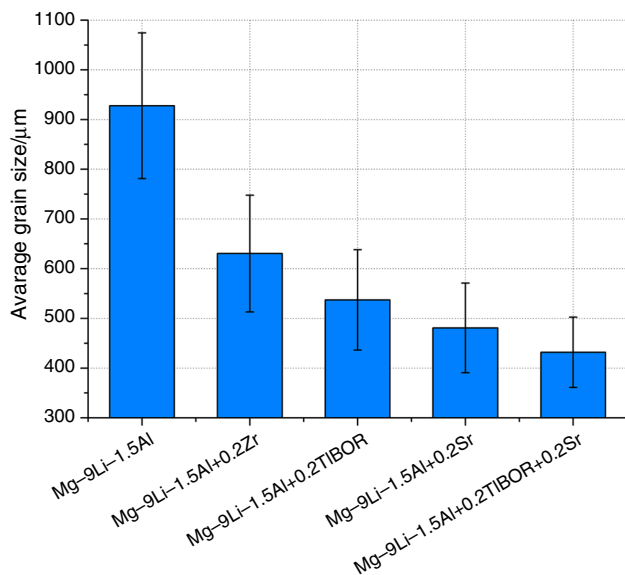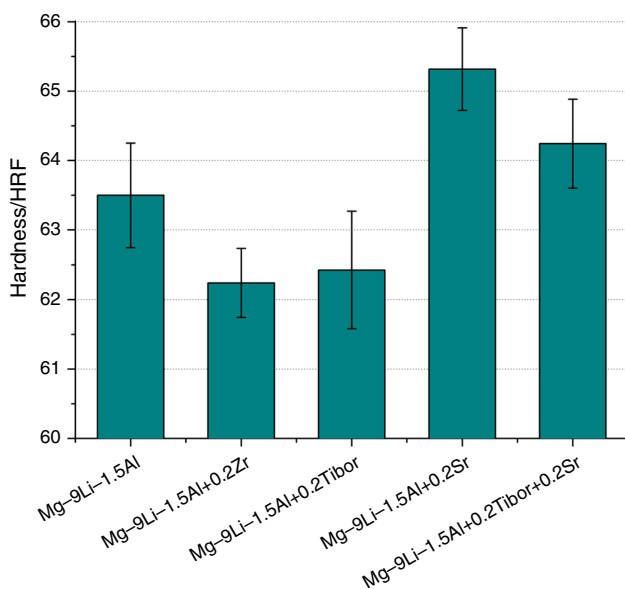
Fig. 4 Grain size of analysed Mg–Li–Al alloys

Fig. 5 Hardness of investigated Mg–9Li–1.5Al alloys

white granular particles of the intermetallic compounds randomly spread in the α and β matrix (Fig. 6b). EDS point analysis carried out on particles (indicated as 3) to determine the chemical composition shows that the mixture consists of high concentration of Zr, Al and Mg elements, which the most probably resulted in the form of Al_3Zr phases as suggested in [21, 22]. With the addition of TiBor master alloy as grain refinement to the Mg–9Li–1.5Al alloy, no other phases are observed in microstructure (Fig. 6c).

Figure 6d, e shows the SEM images and EDS analysis of the Mg–9Li–1.5Al+Sr and Mg–9Li–1.5Al+TiBor+Sr

alloys, respectively. Containing Sr, an element with a larger atomic number, bone-like bright intermetallic compounds (indicated as 3) are situated along the phase boundary as well as across α-phase. EDS point analysis, which was done at location 3, demonstrates the high concentration of Mg, Sr and Mg, Al, Sr, respectively. Considering Al dissolved in the matrix, it can be concluded that these compounds can be related to Al_4Sr or Mg_2Sr as suggested in [6]. Shape and location of recognised phases in analysed alloys could be directly related to the order of nucleation in the intermetallic compounds.

The solidification pathways of as-cast (Fig. 7a) and after modification by 0.2 mass% Zr (Fig. 7b) and 0.2 mass% TiBor (Fig. 7c) and 0.2 mass% AlSr (Fig. 7d) master alloys have been investigated by thermal derivative analysis. Figure 7a shows typical cooling curves and its first derivative curves which were used to determine characteristic points during solidification. For the alloy with 0.2 mass% Zr, only five well-defined points are observed, i.e. at 597.7 °C (1-T_N-nucleation temperature), 578.9 °C (2-T_G-maximum temperature of growth), 526.1 °C (4-T_{SOL}-solidus temperature), 503.3 °C (5-T_S-α+β solvus temperature) and 473.3 °C (6-T_{ER}-end of reactions) as shown in Fig. 7b. No more exothermic peaks were found after modification by Zr that can be corresponded to compounds of Al_3Zr as suggested in [21, 22]. It must be noted that the melting temperature of Al_3Zr intermetallic compound according to the literature [9] is 1580 °C. Results from the thermal derivative analysis (Table 4) present that the addition of 0.2 mass% Zr does not change the nucleation temperature, i.e. 596.5 °C and, however, decreases the solidus temperature from 549.1 °C of investigated magnesium alloys. For both analysed alloys, no significant changes in temperature in other reactions like T_G, T_S and T_{ER} were observed. The solidification time for the cooling rate 0.6 °C s^{-1}, as the difference of the times, at which the liquidus and solidus temperatures occur in Mg–9Li–1.5Al and Mg–9Li–1.5Al+0.2Zr, amounts to $\Delta t = 106$ and 134 s, respectively.

Addition of TiBor and AlSr causes to appearance new well-defined exothermic peak (marked as point 3 in Fig. 7c–e) probably becomes from nucleation of metastable intermetallic phase η(LiAl) with B2 structure [8, 9, 20] 3-$T_{\eta(LiAl)}$ observed at 552.6 °C (Mg–9Li–1.5Al+TiBor), 559.1 °C (Mg–9Li–1.5Al+AlSr) and 546.8 °C (Mg–9Li–1.5Al+0.2TiBor+0.2Sr), however, more studies must be done.

Modification of Mg–9Li–1.5Al alloy by AlSr master alloy causes slight decreases in nucleation temperature to 582.7 °C, but strongly reduces a solidus temperature to 535.3 °C in accordance with the unmodified alloy. The addition of TiBor and AlSr10 master alloys causes

(a)

Point	Element	Wt.%
1	Mg	100
2	Mg	92.5
	Al	7.5

10 µm EHT = 20.00 kV Signal A = QBSD
WD = 9.4 mm Mag = 2.50 K X

(b)

Point	Element	Wt.%
1	Mg	100
2	Mg	92.7
	Al	7.3
3	Mg	13.5
	Al	26.4
	Zr	60.1

20 µm EHT = 20.00 kV Signal A = QBSD
WD = 9.2 mm Mag = 1.00 K X

(c)

Point	Element	Wt.%
1	Mg	100
2	Mg	92.1
	Al	7.9
3	Mg	80.3
	O	5.2
	Al	14.5

10 µm EHT = 20.00 kV Signal A = QBSD
WD = 10.4 mm Mag = 5.00 K X

(d)

Point	Element	Wt.%
1	Mg	100
2	Mg	92.1
	Al	7.9
3	Mg	73.8
	Sr	26.2
4	Mg	75.9
	O	11.8
	Al	12.3

10 µm EHT = 20.00 kV Signal A = QBSD
WD = 11.2 mm Mag = 2.50 K X

(e)

Point	Element	Wt.%
1	Mg	100
2	Mg	94.8
	Al	5.2
3	Mg	85.7
	Sr	11.6
	Al	2.7
4	Mg	71.8
	O	22.9
	Al	5.3

10 µm EHT = 20.00 kV Signal A = QBSD
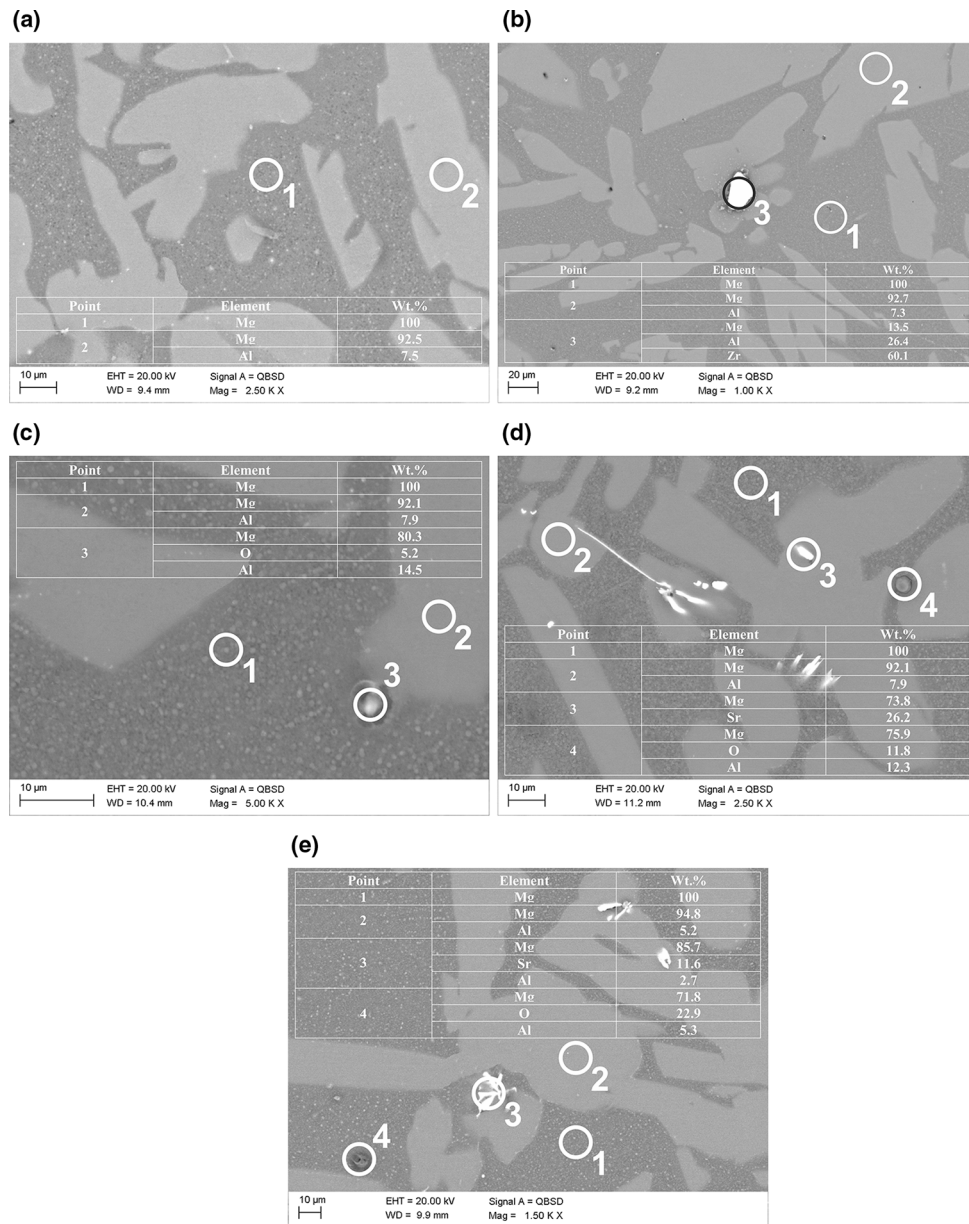WD = 9.9 mm Mag = 1.50 K X

Fig. 6 SEM micrographs with EDS analysis in labelled points of Mg–Li–Al alloys: **a** Mg–9Li–1.5Al, **b** Mg–9Li–1.5Al+0.2Zr, **c** Mg–9Li–1.5Al+0.2TiBor, **d** Mg–9Li–1.5Al+0.2Sr, **e** Mg–9Li–1.5Al+0.2TiBor+0.2Sr

decreases in nucleation temperature and solidus temperature to 579.32 and 520 °C, respectively.

The addition of TiBor and AlSr master alloys increases a crystallisation time to 132 s for Mg–9Li–1.5Al+TiBor, 146 s for Mg–9Li–1.5Al+TiBor and 143 s for Mg–9Li–1.5Al+0.2TiBor+0.2Sr. Moreover, an addition of Sr causes a reduction in a period between the solidus temperature and solvus temperature. Based on thermal derivative analysis, it was found that only addition of TiBor and AlSr simultaneously causes a decrease in temperature of maximum growth of primary β(Li) phase from 581.3 to 575.6 °C.

In general, no exothermic peaks, corresponding to precipitation of Mg_2Sr, with melting temperature 680 °C [8, 9], were observed during analysis of crystallisation process of Mg–Li–Al alloys containing Sr as grain refinement. This may be the causes that the amount of Mg_2Sr intermetallic compound is very low, below the level of detection of the method.

The crystallisation pathway of investigated unmodified and modified magnesium alloys, based on thermal derivative analysis, microstructure investigation, SEM observation and study of binary and ternary systems [8, 9], may be proposed as:
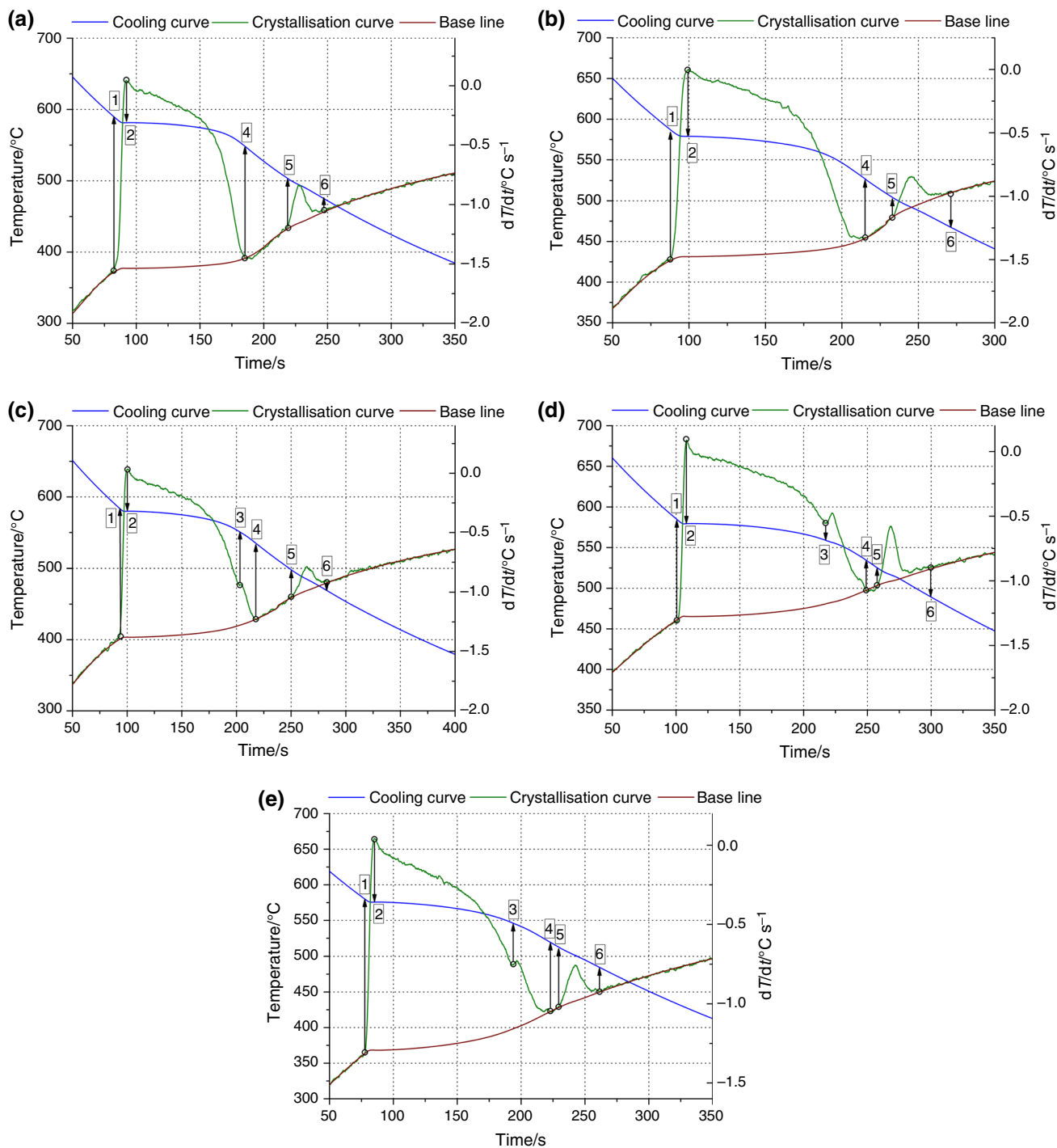
Fig. 7 Representative thermal derivative analysis of investigated Mg–Li–Al alloys: **a** Mg–9Li–1.5Al, **b** Mg–9Li–1.5Al+0.2Zr, **c** Mg–9Li–1.5Al+0.2TiBor, **d** Mg–9Li–1.5Al+0.2Sr, **e** Mg–9Li–1.5Al+0.2TiBor+0.2Sr

1. $L \rightarrow \beta(\mathrm{Li})$
2. Maximum growth of primary $\beta(\mathrm{Li})$-phase
3. $L + \beta(\mathrm{Li}) \rightarrow \alpha(\mathrm{Mg}) + \eta(\mathrm{LiAl})$
4. $\beta(\mathrm{Li}) \rightarrow \alpha(\mathrm{Mg}) + \beta(\mathrm{Li})$

At first, the $\beta(\mathrm{Li})$ (i.e. a solid solution of alloying elements in lithium) starts solidifying, until the liquid

composition reaches the temperature of maximum growth. After passing this point, the phase transition occurs giving $\alpha(\mathrm{Mg})$ phase and $\eta(\mathrm{LiAl})$ intermetallic compound with B2 structure (only for alloys Mg–9Li–1.5Al+0.2TiBor, Mg–9Li–1.5Al+0.2Sr and Mg–9Li–1.5Al+0.2TiBor+0.2Sr). In the last stage of the crystallisation process of investigated Mg–Li–Al alloys, transition in solid state occurs

Table 4 Main reactions during solidification identified by thermal derivative analysis

	1. T_{NUC}/°C	2. T_G/°C	3. $T_{\eta(LiAl)}$/°C	4. T_{SOL}/°C	5. T_S/°C	6. T_{ER}/°C
Mg–9Li–1.5Al	596.5	581.3	–	549.1	505.2	473.9
Mg–9Li–1.5Al+0.2Zr	597.7	578.9	–	526.1	503.3	473.3
Mg–9Li–1.5Al+0.2TiBor	596.3	579.8	552.6	536.4	501.3	466.6
Mg–9Li–1.5Al+0.2Sr	582.7	579.3	559.1	535.3	525.0	473.7
Mg–9Li–1.5Al+0.2TiBor+0.2Sr	579.3	575.6	546.8	520	513.2	474.8

(solvus line in Mg–Li binary system) causing forming of α(Mg) and β(Li) according to reaction β(Li)$\rightarrow$ α(Mg)$+\beta$(Li).

Conclusions

The effects of addition of 0.2 mass% Zr, 0.2 mass% TiBor and 0.2 mass% AlSr grain refiners on the crystallisation process during solidification of the Mg–9Li–1.5Al alloy such as T_N, T_G, T_{SOL}, T_S and T_{ER}, linear coefficient of thermal expansion, microstructure and hardness were studied. The results are summarised as follows:

1. At a 0.6 °C s^{-1} cooling rate, the solidification time of Mg–9Li–1.5Al alloy is increased by adding grain retirements.

2. In analysed material, an addition of Zr does not change T_N, T_G, T_S and T_{ER}; however, decreases T_{SOL}. The addition of TiBor and AlSr causes a reduction in nucleation and solidus temperature.

3. Analysis of the heating and cooling dilatometric curves of analysed materials modified by TiBor and AlSr is characterised by a linear reduction in coefficient of linear thermal expansion as a function of temperature. No transitions in the solid state occur during heating and cooling cycles.

4. The as-cast Mg–9Li–1.5Al alloy comprises α(Mg) and β(Li) phases. AlSr addition results in the formation of new intermetallic compound distributed along the phase boundary as well as across α-phase. EDX analysis shows that the precipitated compounds are Al_4Sr or Mg_2Sr.

5. The addition of Zr, TiBor and AlSr in level 0.2 mass% reduces the grain size of analysed magnesium alloy. The strongest effect in reduction in grain size (grain size decreased almost twice) was achieved when TiBor and AlSr simultaneously were used.

6. Based on hardness measurements, it was found that the addition of AlSr refiner slightly increases hardness. The hardness did not increase with TiBor addition.

7. Thermal derivative analysis can be implemented to registration melting and cooling processes of Mg–Li–Al alloys.

References

1. Liu T, Wu SD, Li SX, Li PJ. Microstructure evolution of Mg-14% Li-1% Al alloy during the process of equal channel angular pressing. Mat Sci Eng A Struct. 2007;460–461:499–503.

2. Wang T, Wu R, Zhang M, Li L, Zhang J, Li J. Effects of calcium on the microstructures and tensile properties of Mg–5Li–3Al alloys. Mat Sci Eng A Struct. 2011;528:5678–84.

3. Mendis CL, Oh-ishi K, Ohkubo T, Hono K. Effect of Li additions on the age hardening response and precipitate microstructures of Mg–2.4Zn–0.16Zr based alloys. Mat Sci Eng A Struct. 2012;535:122–8.

4. Zhanga J, Zhang Y, Wu G, Liu W, Zhanga L, Ding W. Microstructure and mechanical properties of as-cast and extruded Mg–8Li–3Al–2Zn–0.5Nd alloy. Mat Sci Eng A-Struct. 2015;621:198–203.

5. Bao L, Zhang Z, Le Q, Li Q, Cui J. Influence of Gd, Nd and Ce additions on microstructures and mechanical properties of ultralight dual phase Mg–9Li–0.4Zr alloys. Mater Res-Ibero-Am J. 2016;19(3):654–8.

6. Xu T, Peng X, Jiang J, Xie W, Chen Y, Wei G. Effect of Sr content on microstructure and mechanical properties of Mg–Li–Al–Mn alloy. T Nonferr Metal Soc. 2014;24:2752–60.

7. Chenga R, Pana F, Jiang S, Li Ch, Jiang B, Jiang X. Effect of Sr addition on the grain refinement of AZ31 magnesium alloys. Prog Nat Sci-Mater. 2013;23(1):7–12.

8. Goel NC, Cahoon JR. The Al–Li–Mg system (Aluminum–Lithium–Magnesium). Bulletin of Alloy Phase Diagrams. 1990;11:528. https://doi.org/10.1007/BF02841712.

9. A.I.H. Committee, ASM Handbook, volume 3: alloy phase diagrams, 10th ed. ASM International: The Materials Information Company; 1992.

10. Król M, Tański T, Matula G, Snopiński P, Tomiczek AE. Analysis of crystallisation process of cast magnesium alloys based on thermal derivative analysis. Arch Metall Mater. 2015;60(4):2993–9. https://doi.org/10.1515/amm-2015-0478.

11. Król M, Tański T, Sitek W. Thermal analysis and microstructural characterization of Mg–Al–Zn system alloys. Modern Technologies in Industrial Engineering (MODTECH2015), Book Series: IOP Conference Series-Materials Science and Engineering 2015. https://doi.org/10.1088/1757-899x/95/1/012006.

12. Sroka M, Zieliński A, Dziuba-Kałuża M, Kremzer M, Macek M, Jasiński A. Assessment of the residual life of steam pipeline material beyond the computational working time. Metals-Basel. 2017;7(3):82. https://doi.org/10.3390/met7030082.

13. Zieliński A, Sroka M, Miczka M, Śliwa A. Forecasting the particle diameter size distribution in P92 (X10CRWMOVNB9-2) steel after long-term ageing at 600 and 650 & #xB0;C. Arch Metall Mater. 2016;61(2A):753–60. https://doi.org/10.1515/amm-2016-0128.

14. Król M, Tański T, Snopiński P, Tomiczek B. Structure and properties of aluminium–magnesium casting alloys after heat treatment. J Therm Anal Calorim. 2017;127:299–308. https://doi.org/10.1007/s10973-016-5845-4.

15. Meylan B, Terzi S, Gourlay CM, Dahle AK. Dilatancy and rheology at 0–60% solid during equiaxed solidification. Acta Mater. 2011;59:3091–101.

16. Yavari F, Shabestari S. Effect of cooling rate and Al content on solidification characteristics of AZ magnesium alloys using cooling curve thermal analysis. J Therm Anal Calorim. 2017;129(2):655–62.

17. Jafari H, Khalilnezhad M, Farahany S. Computer-aided cooling curve thermal analysis and microstructural evolution of Mg–5Zn–xY cast alloys. J Therm Anal Calorim. 2017;130(3):1429–37.

18. Zovko Brodarac Z, Holjevac Grgurić T, Burja J. Thermodynamic stability of AlSi11 alloy microconstituents. J Therm Anal Calorim. 2017;127(1):431–8.

19. Dutkiewicza J, Rusz S, Maziarz W, Skuza W, Kuc D, Hilser O. Modification of microstructure and properties of extruded Mg–Li–Al alloys of α and α+β phase composition using ECAP processing. Acta Phys Pol A. 2017;131:1303–6.

20. Wu R, Yan Y, Wang G, Murr LE, Han W, Zhang Z, Zhang M. Recent progress in magnesium–lithium alloys. Int Mater Rev. 2015;60(2):65–100.

21. Stjohn DH, Easton MA, Qian M, Taylor JA. Grain refinement of magnesium alloys: a review of recent research, theoretical developments, and their application. Metall Mater Trans A. 2012;44A:2935–49.

22. Friedrich HE, Mordike BL. Magnesium technology metallurgy, design data, applications. Berlin: Springer-Verlag; 2006.